models are more robust than fixed-effect models because they allow simultaneously for variation in effect sizes due to within-study sampling error and between-study variation in effect size (*46*). Repeating analyses using fixed-effect models yielded similar conclusions, except that differences among categories were more likely to be judged significant and fail-safe numbers were much larger.

38. Several lines of evidence suggest that publication bias does not greatly affect the overall pattern identified here. First, scatter plots of effect size versus sample size (Figs. 1 and 3) do not show the pattern suggestive of selective reporting: a funnel with missing values for effect sizes close to zero with small sample sizes (*22*). Second, the rank correlation between effect size and sample size (r_{bias}) for the bird studies was not significantly negative [Spearman rank correlation coefficient (r_S) = −0.26, n = 15 studies, P = 0.32; when the Seychelles warbler was excluded, r_S = −0.39, n = 14 studies, P = 0.17], which would provide evidence for publication bias (*22*). Third, very conservative tests were significant. Taking all bird studies, 13 out of 15 estimates (sign test: P = 0.007, two-tailed), 10 out of 12 species means (sign test: P = 0.039, two-tailed), and 8 out of 9 family means (sign test: P = 0.039, two-tailed) showed positive effect sizes. Fourth, although transformed effect sizes for all studies did not show significant heterogeneity among studies ($\chi^2_{(14)}$ = 10.18, P = 0.75), we also examined the data excluding the study of the Seychelles warblers (*13*), which had the largest effect size, and the largest sample size. Weighted mean effect size was still significantly greater than zero, when studies or species were considered to be independent (Table 1). Fifth, we calculated the number of unpublished studies averaging zero effect size that would have to exist for the overall mean effect size to be not significantly different from zero (Table 1). Interpretation of the meaning of a "fail-safe number" depends in part on subjective assessment of whether it is likely that so many unpublished studies exist (*29*); we consider it unlikely. A quantitative criterion is that a result should be regarded as robust if the fail-safe number, X, exceeds $5n + 10$, where n is the number of studies on which the meta-analyses were based (*29*). By this criterion, none of these results is robust (Table 1), but the sample size is rather small.
39. S. Creel, N. M. Creel, S. L. Monfort, *Anim. Reprod. Sci.* **53**, 315 (1998).
40. B. H. King, *Oecologia* **78**, 420 (1989).
41. E. L. Charnov, R. L. Los-den Hartogh, W. T. Jones, J. van den Assem, *Nature* **289**, 27 (1981).
42. I. Pen, F. J. Weissing, S. Daan, *Am. Nat.* **153**, 384 (1999).
43. _____, *Nature* **329**, 627 (1987).
44. E. A. Herre, C. A. Machado, S. A. West, in *Adaptionism and Optimality*, S. Orzack, E. Sober, Eds. (Cambridge Univ. Press, Cambridge, 2001), pp. 191–218.
45. Consistent with the predicted importance of the strength and form of selection; (i) fig wasp species show more extreme sex ratio shifts in more variable environments, where there is stronger selection to adjust sex ratios in response to environmental conditions (*43*, *44*), and more precise (lower variance) sex ratios in situations where selection for precise sex ratios (stabilizing selection) is greater (*47*); (ii) in species where the method of sex determination may impose a heavy constraint (such as CSD and pseudo-arrhenotoky in spiders, aphids, snakes, and mites), many cases of extreme (and precise) sex ratio variation occur when there is intense competition among brothers for mates (local mate competition) and strong selection for extremely female-biased sex ratios (such as 5% males) (*12*, *14*, *48*, *49*); and (iii) environmental predictability could be important in explaining broad taxonomic patterns, because in many cases it would seem likely to be easier for insects such as parasitic wasps to assess relevant factors than for a vertebrate to do so (*11*).
46. J. Gurevitch, L. V. Hedges, *Ecology* **80**, 1142 (1999).
47. S. A. West, E. A. Herre, *Evolution* **52**, 475 (1998).
48. Y. Yamaguchi, *Nature* **318**, 460 (1985).
49. C. J. Nagelkerke, M. W. Sabelis, *J. Evol. Biol.* **11**, 649 (1998).

50. We thank D. Allsop, F. Balloux, N. Colegrave, A. Griffin, K. Lessells, I. Pen, S. Reece, L. Rowe, D. Shuker, and A. Sugden for useful discussion; and J. van Alphen, R. Belshaw, G. Broad, C. Godfray, J. Noyes, A. Rivero, and especially D. Quicke for supplying biological and taxonomic help. Funded by the UK Biotechnology and Biological Sciences Research Council, the National Environment Research Council (UK), and the Royal Society.

17 December 2001; accepted 24 January 2002
Published online 31 January 2002;
10.1126/science.1069043
Include this information when citing this paper.

Extraction of Black Hole Rotational Energy by a Magnetic Field and the Formation of Relativistic Jets

Shinji Koide,[1] Kazunari Shibata,[2] Takahiro Kudoh,[3] David L. Meier[4]

Using numerical simulations, we modeled the general relativistic magnetohydrodynamic behavior of a plasma flowing into a rapidly rotating black hole in a large-scale magnetic field. The results show that a torsional Alfvén wave is generated by the rotational dragging of space near the black hole. The wave transports energy along the magnetic field lines outward, causing the total energy of the plasma near the hole to decrease to negative values. When this negative energy plasma enters the horizon, the rotational energy of the black hole decreases. Through this process, the energy of the spinning black hole is extracted magnetically

Relativistic jets have now been discovered in several different classes of astrophysical objects, including active galactic nuclei (*1*, *2*), microquasars (*3*, *4*), and gamma ray bursts (*5*). A rapidly spinning black hole may exist at the center of each of these objects, and energetic reactions that occur near the hole may be responsible for the jets. One of the most promising processes for producing relativistic jets is the extraction of rotational energy from a spinning (Kerr) black hole (*6*, *7*). One method of extraction is the Penrose process, which uses fission of a particle near the black hole to extract the black hole rotational energy (*6*). However, this process may not be applicable to most astrophysical objects, because the particle fission must occur near the black hole, and the relative velocity of the particles produced by the fission should be near the speed of light. On the other hand, Blandford and Znajek (*7*) showed that a large-scale magnetic field around a Kerr black hole also could extract rotational energy. They assumed a magnetic force–free condition, which corresponds to an extremely strong magnetic field or an extremely low inertia plasma case. Recently, evidence of the extraction of rotational energy from a Kerr black hole by a magnetic field was suggested by observations of a broad Fe Kα line in the bright Seyfert 1 galaxy MCG-6-30-15 (*8*). Modeling of this emission indicates that it is concentrated in a small central disk region near the black hole. It is plausibly explained by a model in which the black hole rotational energy is being extracted into the disk by a magnetic field with a strength of $\sim 10^4$ Gauss that connects the black hole to the disk.

To understand the basic physics of rotational energy extraction from a black hole with a finite magnetic field, we have investigated a somewhat simpler system using general relativistic magnetohydrodynamic (MHD) numerical calculations. Initially, the system consists of a Kerr black hole with a uniform magnetic field, uniform plasma, and no accretion disk. The calculations are based on the general relativistic formulation of the laws of conservation of particle number and

[1]Faculty of Engineering, Toyama University, 3190 Gofuku, Toyama 930–8555, Japan. [2]Kwasan and Hida Observatory, Kyoto University, Yamashina, Kyoto, 607–8471, Japan. [3]National Astronomical Observatory, Mitaka, Tokyo 181–8588, Japan. [4]Jet Propulsion Laboratory, California Institute of Technology, Pasadena, CA 91109, USA.

energy momentum, Maxwell equations, and Ohm's law with zero electrical resistance (*9*–*11*). Here, we neglect the radiation cooling effect. We use the Kerr metric, which describes the curved space-time around a spinning black hole. Such a black hole has two characteristic parameters, mass M and angular momentum J. We use the normalized rotation parameter $a = J/J_{max}$, where $J_{max} = GM^2/c$ is the maximum angular momentum of a Kerr black hole, G is the gravitational constant, and c is the speed of light. We set $a = 0.99995$, which corresponds to a nearly maximally rotating black hole. Around the hole, we initialize the plasma to a uniform mass density ρ_0 and low pressure $p_0 = 0.06\rho_0 c^2$. The initial momentum of the plasma is zero everywhere, and the initial magnetic field is also uniform (*12*, *13*) and strong, ${B_0}^2 = 10\rho_0 c^2$. This is the magnetic field–dominated case, with the Alfvén velocity $v_A = 0.953c$, close to the speed of light. To calculate the time evolution of the plasma around the black hole, we use a simplified total variable diminishing (TVD) difference scheme with 3+1 formalism of the general relativistic MHD equations, in which special (three components) and time (one component) derivatives are separated completely (*9*). We assume axisymmetry with respect to the z axis and reflection symmetry with respect to the equatorial plane. We perform simulations in the region $0.51\ r_S < r < 20\ r_S$ and $0.01 < \theta < \pi/2$, where r and θ are the radial and co-latitude coordinates, respectively, and $r_S = 2GM/c^2$ is the Schwarzschild radius of the black hole.

The time evolution of the system (Fig. 1) shows that at $t = \tau_S = r_S/c$, the plasma begins to fall into the black hole (Fig. 1B) (where t is time and τ_S is unit of time). The azimuthal component of the magnetic field has begun to increase because of the azimuthal twisting of the magnetic field lines. This is a general relativistic effect in which the rotating black hole drags the space (inertial frame) around it. The frame-dragging effect produces a special region called the ergosphere, in which any material, information, or energy must rotate in the same direction as the black hole. Under the assumption of infinite electrical conductivity, the plasma cannot cross the magnetic field lines; it can only flow parallel to them. That is, the magnetic field lines are tied to the plasma or frozen in. The magnetic field lines then are twisted azimuthally in the direction of the black hole rotation by the rotation of the plasma in the ergosphere. This effect is similar to a dynamo effect in the broad sense, called the Ω effect in the dynamo theory of geomagnetism, and therefore called the frame-dragging dynamo (*14*, *15*). At $t = 7\ \tau_S$, this process has amplified the magnetic field to a value that is three times larger than the initial magnetic field strength in the ergosphere (Fig. 1D). The twist of the magnetic field lines propagates outward along the magnetic field lines against the infalling plasma flow as a torsional Alfvén wave (Fig. 1, B through D). This production of a torsional Alfvén wave is also found in nonrelativistic simulations of magnetized accretion disks in Keplerian orbital rotation about normal stars (*16*–*20*).

To portray the result more intuitively, we show in three dimensions the magnetospheric structure around the Kerr black hole at $t = 7\ \tau_S$ (Fig. 2). At this time, the black hole has rotated more than once since the beginning of the simulation. The magnetic field lines that cross the ergosphere surface are twisted azimuthally, whereas the magnetic field lines that do not cross the ergosphere surface are twisted only weakly and are slightly bent toward the black hole by the falling plasma. Those around the equatorial plane inside the ergosphere are bent azimuthally in the same direction as the black hole rotation. Magnetic field lines have tension similar to that of a rubber band or a bowstring, so in the region the magnetic tension torques the plasma in a direction opposite to that of the black hole rotation. If we define the sign of the angular momentum of the black hole to be positive, then the magnetic tension causes the angular momentum of the plasma in the ergosphere to become negative. Therefore, the angular momentum of the plasma in the region outside the ergosphere receives a net increase, because the total angular momentum of the whole plasma around the black hole (initially zero) must be conserved. This redistribution of plasma angular momentum is a consequence of the magnetic field lines threading the rotating space.

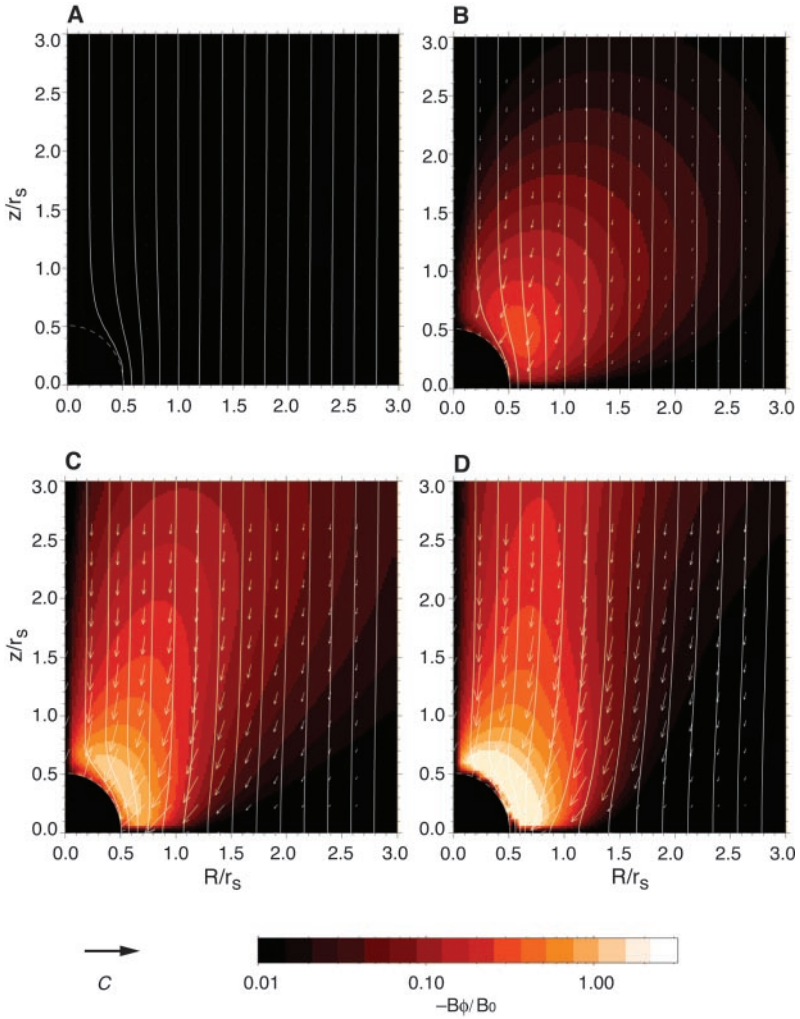

Fig. 1. Time evolution of a simple system of a large-scale magnetic field, thin plasma, and a Kerr black hole at (**A**) $t = 0$, (**B**) $t = 1\ \tau_S$, (**C**) $t = 4\ \tau_S$, and (**D**) $t = 7\ \tau_S$. The color shows the value of $-B_\phi/B_0$, where B_ϕ is the azimuthal component of the magnetic field. The arrows show the poloidal velocity of the plasma. Solid lines are magnetic field lines (surfaces). The black quarter-circle at the origin indicates the event horizon of the black hole (the event horizon is the boundary of a black hole, through which no information, material, or energy can pass outward), whose radius is $r_H = r_S(1 + \sqrt{1 - a^2})/2 = 0.505\ r_S$. The dotted line shows the inner boundary of the calculation region at $r = 1.01\ r_H$.

Energy is transported in this system by the large-scale magnetic field (Fig. 3). The quantity plotted, called the energy at infinity, is the total energy and corresponds to the sum of rest mass energy, kinetic energy, thermal energy, gravitational energy, and electromagnetic energy, and is one of the globally conservative quantities around a Kerr black hole. Outside of the ergosphere, this energy is always positive because it includes the rest mass energy, but inside it may become negative because of the frame-dragging effect if the plasma has negative, relativistic angular momentum. The electromagnetic energy flux density shows that, even though the plasma is falling into the black hole, electromagnetic energy is ejected along the magnetic field lines from the ergosphere (Fig. 3). This outward flow of electromagnetic energy is due to propagation of the Alfvén wave against the plasma infall; we call the region of outflowing electromagnetic energy the Alfvén wave region. Integrating the electromagnetic flux over the surface of the cylinder $R = r \sin\theta \leq 0.8\, r_S$, $-r_S \leq z \leq r_S$, we find the electromagnetic power of the Alfvén wave to be $L_{EM} \sim 0.39\, B_0^2 r_S^2 c/\mu_0$, where μ_0 is magnetic permeability. On the other hand, hydrodynamic energy is transported toward the black hole with a rate $L_{hyd} \sim -0.29\, B_0^2 r_S^2 c/\mu_0$, so the net energy flux from the ergosphere is $L_{tot} = L_{EM} + L_{hyd} \sim 0.10\, B_0^2 r_S^2 c/\mu_0$. This flux is so large that, for material at the foot point of the Alfvén wave region, the energy at infinity becomes negative (Fig. 3), causing the plasma there to fall rapidly into the black hole. We call this region the negative energy–falling region. Between the Alfvén wave region and the negative energy–falling region, there is an important area we call the frame-dragging dynamo region. Here the kinetic energy of the plasma is converted into the electromagnetic free energy by the frame-dragging dynamo effect, increasing the strength of the azimuthal magnetic field component. The energy transport through these three regions can be summarized as follows. Because of the outward propagation of the electromagnetic free energy (against the plasma inflow) in the Alfvén wave region, the energy at infinity decreases to a negative value, and plasma with the negative energy at infinity subsequently falls into the black hole. When the negative energy plasma is swallowed by the black hole, the rotation energy of the Kerr black hole decreases. So the ultimate result of the generation of an outward Alfvén wave is the magnetic extraction of rotational energy of the Kerr black hole. This is a consistent solution showing the extraction mechanism of the Kerr black hole rotation energy by the finite strength magnetic field. In the Penrose process, an elementary particle reaction redistributes the angular momentum of particles into orbits with negative energy at infinity. Our simulation shows that the large-scale magnetic field plays the same role. Therefore, we shall call the extraction of rotational energy that we see in our simulation the MHD Penrose process (*21–23*). This MHD Penrose process is transient and may settle down to a steady state after long-term simulation. Unfortunately, we cannot discuss this point because the simulation stops at $t = 7\,\tau_S$ because of a code problem. New codes are being constructed at the present time to allow longer-term simulations.

When the outflowing electromagnetic energy reaches the gravity-free region far from the black hole ($r \gg r_S$), it may be converted to kinetic energy by MHD mechanisms (*24*). This would result in the formation of a jet with Lorentz factor $\Gamma = 1 + B_\phi^2/(2\,\mu_0 \rho c^2)$. This scenario is similar to the ergosphere-driven wind model of Punsly and Coroniti (*25*), but that paper did not discuss the most important points of the process: the relation to the Penrose process and the nonsteady infalling of plasma with the negative energy at infinity caused by the magnetic field into the black hole. Punsly and Coroniti estimated

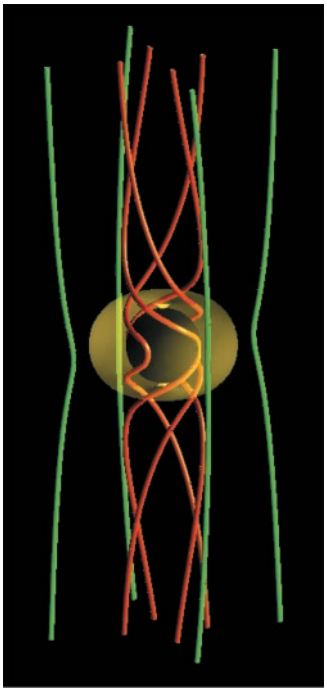

Fig. 2. Three-dimensional graphics of magnetic field lines around a Kerr black hole at $t = 7\,\tau_S$. The black sphere at the center depicts the black hole. The yellow surface around the black hole is that of the ergosphere, inside which any material, information, or energy must rotate in the same direction as the black hole. The shape of the surface is like that of an apple in this high rotation parameter case ($a \sim 1$), with a cusp-like dimple at the top and bottom: At the pole it touches the horizon $r = r_H$ and on the equatorial plane, the radius is r_S. (In the low rotation parameter case, $a < 0.8$, the shape is like an ellipsoid.) The red tubes show the magnetic field lines that cross into the ergosphere and the green lines show those that do not.

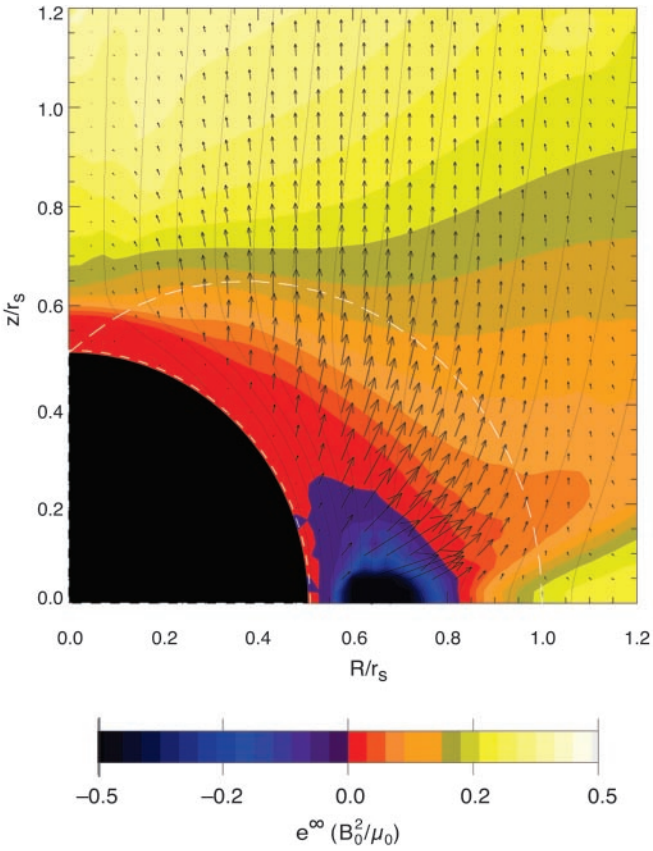

Fig. 3. Energy transport in the simple system of a large-scale magnetic field, thin plasma, and a Kerr black hole at $t = 7\,\tau_S$. The black region indicates the black hole horizon, and the short-dashed line shows the inner boundary of the calculation region ($r = 1.01\, r_H$). The long-dashed line indicates the boundary of the ergosphere. The thin solid line is the magnetic field line (surface). The color shows the density of the energy at infinity. The arrows show the electromagnetic energy flux density.

the electromagnetic power from the ergosphere wind to be comparable to that coming directly from the rapidly rotating black hole's horizon by the Blandford-Znajek mechanism (*7*): $L_{BZ} \sim (\pi/4)(a^2c/v_A)B_0^2 r_H^2 c/\mu_0$. The total electromagnetic power from the spinning black hole then would be $L_{EM} \sim 2\ L_{BZ} \sim (\pi/2)(a^2c/v_A)B_0^2 r_H^2 c/\mu_0 \sim 0.4\ B_0^2 r_S^2 c/\mu_0$, which is consistent with the value we obtained from our numerical simulation ($L_{EM} \sim 0.39\ B_0^2 r_S^2 c/\mu_0$).

The process may be applicable to the formation of jets from active elliptical galaxies such as M87. Such galaxies typically have small amounts of gas and dust, and a tenuous accretion disk will form around the central black hole. In this case, the power generated by the magnetic mechanism of the jet formation driven by rotation of a Kerr black hole may be comparable to that of the accretion disk (*26*). The MHD Penrose process also may be related to gamma-ray bursts (*27*). Plasma in the polar regions of the ergosphere will fall directly into the black hole, forming a low-density region there. An outgoing Alfvén wave will be generated in the same polar region. When we consider a strong magnetic field ($B_0 = 10^{15}$ Gauss) around a stellar-mass [$M = 10\ M_{sun}$, where M_{sun} is the solar mass ($M_{sun} = 2 \times 10^{30}$ kg)], extremely rapidly rotating ($a = 1$), Kerr black hole, the power of the Alfvén wave is estimated to be $L_{EM} \sim 4 \times 10^{52}$ erg/s, which is similar to the power seen in gamma-ray bursts. The power is on the same order as the estimation based on the Blandford-Znajek mechanism (*28*). Furthermore, if the Alfvén wave is converted into plasma kinetic energy by some mechanism (*24*), it would produce a relativistic jet with a small amount of baryons, which also is required to produce a gamma-ray burst event.

References and Notes

1. T. J. Pearson *et al.*, *Nature* **290**, 365 (1981).
2. J. A. Biretta, W. B. Sparks, F. Macchetto, *Astrophys. J.* **520**, 621 (1999).
3. I. F. Mirabel, L. F. Rodriguez, *Nature* **371**, 46 (1994).
4. S. J. Tingay *et al.*, *Nature* **374**, 141 (1995).
5. S. R. Kulkarni *et al.*, *Nature* **398**, 389 (1999).
6. R. Penrose, *Nuovo Cimento* **1**, 252 (1969).
7. R. D. Blandford, R. Znajek, *Mon. Not. R. Astron. Soc.* **179**, 433 (1977).
8. J. Wilms *et al.*, *Mon. Not. R. Astron. Soc.*, **328**, 627(2001).
9. S. Koide, K. Shibata, T. Kudoh, *Astrophys. J.* **495**, L63 (1998).
10. ———, *Astrophys. J.* **522**, 727 (1999).
11. S. Koide, D. L. Meier, K. Shibata, T. Kudoh, *Astrophys. J.* **536**, 668 (2000).
12. R. M. Wald, *Phys. Rev. D* **10**, 1680 (1974).
13. We use the magnetic field from the Wald solution (*12*) for the initial condition, and the electric field is determined by the ideal MHD condition.
14. M. Yokosawa, *Publ. Astron. Soc. Jpn.* **45**, 207 (1993).
15. D. L. Meier, *Astrophys. J.* **522**, 753 (1999).
16. Y. Uchida, K. Shibata, *Publ. Astron. Soc. Jpn.* **37**, 515 (1985).
17. K. Shibata, Y. Uchida, *Publ. Astron. Soc. Jpn.* **38**, 631 (1986).
18. R. Ouyed, R. E. Pudritz, J. M. Stone, *Nature* **385**, 409 (1997).
19. T. Kudoh, R. Matsumoto, K. Shibata, *Astrophys. J.* **508**, 186 (1998).
20. D. L. Meier, S. Koide, Y. Uchida, *Science* **291**, 84 (2001).
21. M. Takahashi, S. Nitta, Y. Tatematsu, A. Tomimatsu, *Astrophys. J.* **363**, 206 (1990).
22. K. Hirotani, M. Takahashi, S.-Y. Nitta, A. Tomimatsu, *Astrophys. J.* **386**, 455 (1992).
23. D. L. Meier, *Astrophys. J.* **548**, L9 (2001).
24. T. Kudoh, K. Shibata, *Astrophys. J.* **514**, 493 (1999).
25. B. Punsly, F. V. Coroniti, *Astrophys. J.* **354**, 583 (1990).
26. R. D. Blandford, D. Payne, *Mon. Not. R. Astron. Soc.* **199**, 883 (1982).
27. A. I. MacFadyen, S. E. Woosley, A. Heger, *Astrophys. J.* **550**, 410 (2001).
28. R. Pophan, S. E. Woosley, C. Fryer, *Astrophys. J.* **518**, 356 (1999).

29. We thank M. Koide, K. Hirotani, and R. Blandford for comments and discussion for this study. We appreciate the support of the National Institute for Fusion Science and National Astronomical Observatory of Japan in the use of their super computers and special devices for display. Supported in part by the Scientific Research Fund of the Japanese Ministry of Education, Culture, Sports, Science, and Technology and Research and Development for Applying Advanced Computational Science and Technology, the Japan Science and Technology Corporation. Some of this research was carried out at the Jet Propulsion Laboratory, California Institute of Technology, under contract to NASA.

20 November 2001; accepted 16 January 2002
Published online 24 January 2002;
10.1126/science.1068240
Include this information when citing this paper.

Quantum Impurities in the Two-Dimensional Spin One-Half Heisenberg Antiferromagnet

O. P. Vajk,[1] P. K. Mang,[2] M. Greven,[2,3]* P. M. Gehring,[4] J. W. Lynn[4]

The study of randomness in low-dimensional quantum antiferromagnets is at the forefront of research in the field of strongly correlated electron systems, yet there have been relatively few experimental model systems. Complementary neutron scattering and numerical experiments demonstrate that the spin-diluted Heisenberg antiferromagnet $La_2Cu_{1-z}(Zn,Mg)_zO_4$ is an excellent model material for square-lattice site percolation in the extreme quantum limit of spin one-half. Measurements of the ordered moment and spin correlations provide important quantitative information for tests of theories for this complex quantum-impurity problem.

The field of low-dimensional quantum magnetism has been of enormous interest to the condensed-matter physics community ever since the discovery that La_2CuO_4, the parent compound of the original high-temperature superconductor $(La,Ba)_2CuO_4$, is a model two-dimensional (2D) quantum (spin-1/2) antiferromagnet. Because the superconductivity occurs in the vicinity of an antiferromagnetic phase in these materials, it appears likely that antiferromagnetic fluctuations are at least partially responsible for their rich physics. One of the new frontiers in condensed-matter physics lies in the field of quantum critical behavior, especially of "dirty" low-dimensional systems involving quantum impurities (*1*). Although there has been much progress in the experimental investigation of quantum impurities in the simpler 1D $S = 1/2$ chain (*2*) and ladder compounds (*3*), experiments with the 2D analog have been restricted to low-impurity concentrations because of the lack of suitable samples (*4*–*7*).

We have investigated the properties of the spin-1/2 square-lattice Heisenberg antiferromagnet (SLHAF) in the presence of a significant density z of quenched, spinless quantum impurities, up to and through the percolation threshold. Specifically, the combined experimental and numerical results for the ordered moment $M_{st}(z)$ and spin correlations $\xi(z,T)$ demonstrate that $La_2Cu_{1-z}(Zn,Mg)_zO_4$ is well described by the Hamiltonian

$$\mathcal{H} = J \sum_{\langle i,j \rangle} p_i p_j \mathbf{S}_i \cdot \mathbf{S}_j, \qquad (1)$$

where the sum is over nearest-neighbor (NN) sites, J is the antiferromagnetic Cu-O-Cu superexchange, $\mathbf{S}_i$ is the $S = 1/2$ operator at site i, $p_i = 1$ on magnetic sites, and $p_i = 0$ on nonmagnetic sites.

In the absence of quantum fluctuations, the NN square lattice undergoes a geometric transition with site dilution z at the percolation threshold $z_p \approx 40.725\%$ (*8*, *9*). As indicated in Fig. 1, below this concentration there is always one cluster of connected sites that spans the infinite lattice. Above z_p, the lattice consists entirely of finite-sized clusters. In studies of site-diluted $S = 5/2$ Heisenberg

[1]Department of Physics, [2]Department of Applied Physics, Stanford University, Stanford, CA 94309, USA. [3]Stanford Synchrotron Radiation Laboratory, Stanford, CA 94305, USA. [4]NIST Center for Neutron Research, National Institute of Standards and Technology, Gaithersburg, MD 20899, USA.

*To whom correspondence should be addressed. E-mail: greven@stanford.edu

Extraction of Black Hole Rotational Energy by a Magnetic Field and the Formation of Relativistic Jets

Shinji Koide, Kazunari Shibata, Takahiro Kudoh, and David L. Meier

Science **295** (5560), . DOI: 10.1126/science.1068240